The G-protein–gated K+ channel, IKACh, is required for regulation of pacemaker activity and recovery of resting heart rate after sympathetic stimulation

The G-protein–gated K^+ channel, I_{KACh}, is required for regulation of pacemaker activity and recovery of resting heart rate after sympathetic stimulation

Pietro Mesirca,[1,2,3] Laurine Marger,[1,2,3] Futoshi Toyoda,[4] Riccardo Rizzetto,[1,2,3] Matthieu Audoubert,[1,2,3] Stefan Dubel,[1,2,3] Angelo G. Torrente,[1,2,3] Mattia L. DiFrancesco,[1,2,3] Jana Christina Muller,[1,2,3] Anne-Laure Leoni,[5] Brigitte Couette,[1,2,3] Joël Nargeot,[1,2,3] David E. Clapham,[6,7,8] Kevin Wickman,[9] and Matteo E. Mangoni[1,2,3]

[1]Centre National de la Recherche Scientifique (CNRS) UMR 5203, Institut de Génomique Fonctionnelle, Département de Physiologie, Laboratoire d'Excellence Canaux Ioniques d'Intérêt Thérapeutique, 34094 Montpellier, France
[2]Institut National de la Santé et de la Recherche Médicale (INSERM) U661, 34094 Montpellier, France
[3]Universités de Montpellier 1 & 2, 34094 Montpellier, France
[4]Department of Physiology, Shiga University of Medical Science, Otsu, Shiga 520-2192, Japan
[5]INSERM UMR 1087, CNRS UMR 6291, l'institut du thorax, Université de Nantes, 44007 Nantes, France
[6]Howard Hughes Medical Institute and [7]Manton Center for Orphan Disease Research, Boston Children's Hospital, Boston, MA 02115
[8]Department of Neurobiology, Harvard Medical School, Boston, MA 02115
[9]Department of Pharmacology, University of Minnesota, Minneapolis, MN 55455

Parasympathetic regulation of sinoatrial node (SAN) pacemaker activity modulates multiple ion channels to temper heart rate. The functional role of the G-protein–activated K^+ current (I_{KACh}) in the control of SAN pacemaking and heart rate is not completely understood. We have investigated the functional consequences of loss of I_{KACh} in cholinergic regulation of pacemaker activity of SAN cells and in heart rate control under physiological situations mimicking the fight or flight response. We used knockout mice with loss of function of the Girk4 (Kir3.4) gene ($Girk4^{-/-}$ mice), which codes for an integral subunit of the cardiac I_{KACh} channel. SAN pacemaker cells from $Girk4^{-/-}$ mice completely lacked I_{KACh}. Loss of I_{KACh} strongly reduced cholinergic regulation of pacemaker activity of SAN cells and isolated intact hearts. Telemetric recordings of electrocardiograms of freely moving mice showed that heart rate measured over a 24-h recording period was moderately increased (10%) in $Girk4^{-/-}$ animals. Although the relative extent of heart rate regulation of $Girk4^{-/-}$ mice was similar to that of wild-type animals, recovery of resting heart rate after stress, physical exercise, or pharmacological β-adrenergic stimulation of SAN pacemaking was significantly delayed in $Girk4^{-/-}$ animals. We conclude that I_{KACh} plays a critical role in the kinetics of heart rate recovery to resting levels after sympathetic stimulation or after direct β-adrenergic stimulation of pacemaker activity. Our study thus uncovers a novel role for I_{KACh} in SAN physiology and heart rate regulation.

The Journal of General Physiology

INTRODUCTION

Cardiac pacemaker activity is tightly regulated by the autonomic nervous system. The sympathetic nervous system enhances heart rate and contractility, whereas the parasympathetic (vagal) inputs slow pacemaking. The dominant pacemaker region of the heart, the sinoatrial node (SAN), is innervated by a rich and complex network of vagal nerve endings (Pauza et al., 1999, 2000). Parasympathetic regulation of SAN pacemaker activity is initiated when vagally released acetylcholine (ACh) binds to muscarinic M_2 receptors, which promotes dissociation of βγ subunit complexes, leading to direct opening of the G-protein–gated inwardly rectifying K^+ channel (Girk/Kir) I_{KACh} (Krapivinsky et al., 1995; Wickman et al., 1999). Activation of muscarinic receptors negatively regulates other ion channels involved in heart automaticity, such as hyperpolarization-activated f (hyperpolarization-activated cyclic nucleotide–gated channel [HCN])-channels underlying the I_f current (DiFrancesco, 2010) and L-type Ca^{2+} channels ($I_{Ca,L}$; Petit-Jacques et al., 1993; Zaza et al., 1996; Mangoni and Nargeot, 2008), as well as ryanodine receptor–mediated Ca^{2+} release (Lakatta et al., 2010). All of these ionic mechanisms are thus potentially involved in the cholinergic regulation

Correspondence to Matteo E. Mangoni: matteo.mangoni@igf.cnrs.fr

Abbreviations used in this paper: ACh, acetylcholine; bpm, beats per minute; ECG, electrocardiogram; Girk, G-protein–gated inwardly rectifying K^+ channel; HRV, heart rate variability; ISO, isoproterenol; MDP, maximum diastolic potential; SAN, sinoatrial node.

The Rockefeller University Press $30.00
J. Gen. Physiol. Vol. 142 No. 2 113–126
www.jgp.org/cgi/doi/10.1085/jgp.201310996

of heart rate, but their relative importance is still a matter of debate (Mangoni and Nargeot, 2008).

I_{KACh} is strongly expressed in the SAN, atria, and atrioventricular node (Giles and Noble, 1976; Noma and Trautwein, 1978; Löffelholz and Pappano, 1985; DiFrancesco et al., 1989; Lomax et al., 2003). Neuronal and cardiac Girk channels are homo- and heterotetrameric complexes formed by subunits encoded by four genes named Girk1–4 (Kir3.1–4; Wickman and Clapham, 1995). The heart expresses Girk1 and Girk4 genes (Wickman et al., 1999; Dobrzynski et al., 2001), and cardiac I_{KACh} channels are complexes consisting of Girk1 and Girk4 (Wickman et al., 1999). However, the Girk1 subunit requires coexpression of another Girk subunit to be targeted at the cell membrane (Kennedy et al., 1999). Consequently, ablation of Girk4 subunits in mice leads to a complete loss of I_{KACh} current in atrial myocytes (Wickman et al., 1998).

The heart rate of Girk4 knockout mice ($Girk4^{-/-}$) shows reduced variability and a diminished responsiveness to pharmacological stimulation of the baroreflex and adenosine receptors (Wickman et al., 1998). However, the physiological effects of Girk4 inactivation on the SAN I_{KACh} and on the cholinergic regulation of SAN pacemaking have not been investigated. Here we show that Girk4 inactivation abolished SAN I_{KACh} and reduced cholinergic regulation of pacemaker activity in isolated SAN cells and intact hearts. In $Girk4^{-/-}$ mice, I_{KACh} was required for normal recovery of resting heart rate after stress, physical exercise, or direct pharmacological stimulation of pacemaking via β-adrenergic receptors. Our study analyzes the impact of I_{KACh} loss of function in the cholinergic regulation of SAN pacemaking and uncovers a previously unexpected role for this channel in heart rate regulation.

MATERIALS AND METHODS

The investigation conforms to the European directives (86/609/CEE) and the Guide for the Care and Use of Laboratory Animals published by the U.S. National Institutes of Health (NIH publication no. 85-23, revised 1996). The French Ministry of Agriculture and the local Ethical Committee of the University of Montpellier 1 & 2 approved all procedures with animals.

$Girk4^{-/-}$ mouse strain

Before starting the study, we obtained experimental $Girk4^{-/-}$ animals by crossing mice from the original mutant colony (Wickman et al., 1998) with mice of C57B6/J genetic background from Charles River in the free of specific pathogenic organisms (EOPS) animal facility of the Réseau d'Animalèrie de Montpellier (RAM) at the Institut de Génetique Humaine (Montpellier, France). We next backcrossed the offspring for 10 generations on C57B6/J mice before starting the study. Animals were given ad libitum access to food and drinking water and were maintained in a 12-h light–dark cycle (light, 8:30 a.m. to 8:30 p.m.).

Staining of SAN tissue and image analysis

We used isolated mouse atrio-nodal (SAN-atrium) preparations in which the right atrium remained intact with SAN to facilitate orientation determination and to preserve tissue integrity. WT and $Girk4^{-/-}$ mice were dissected and placed immediately into 4% paraformaldehyde for 20 min at room temperature, followed by soaking in 1× PBS for several hours. The tissue was suspended in 250 µl of 2% BSA (Sigma-Aldrich), 500 µg/ml digitonin (Sigma-Aldrich) containing an anti-HCN4 monoclonal antibody (1:100 rat, SHG 1E5; Santa Cruz Biotechnology, Inc.), anti-Girk4 polyclonal antibody (1:100 goat, A-14; Santa Cruz Biotechnology, Inc.), or anti-Girk1 polyclonal antibody (1:100 rabbit, H-145; Santa Cruz Biotechnology, Inc.), and 0.002% Na azide to prevent bacterial growth. Tissues were incubated for 66 h at room temperature with very gentle shaking in a Lab-Tek II chamber slide (Thermo Fisher Scientific). The tissue was rinsed 5 × 500 µl (1× PBS) over a 5-h period at room temperature. The procedure was repeated again, but this time the tissue was incubated with chicken anti–rat Alexa Fluor 647 (1:500; Molecular Probes), donkey anti–goat Alexa Fluor 568 (1:500; Molecular Probes), and donkey anti–rabbit Alexa Fluor 488 secondaries (1:500; Molecular Probes). The tissue was placed in ProLong Gold (Invitrogen), and a portion of the right atrium was removed and discarded to simplify mounting of the sample. A glass coverslip was gently placed over the sample with the epicardial side face up. Images were taken with a confocal microscope (TCS LSI; Leica) at the Montpellier RIO Imaging facility of the Arnaud de Villeneuve Campus. Analysis of images was performed with the JaCoP plugin for ImageJ (National Institutes of Health; Bolte and Cordelières, 2006). Appropriate threshold levels were manually adjusted, and the Manders coefficient of colocalization between HCN4 and Girk4, as well as between HCN4 and Girk1 was calculated using JaCoP software.

Isolation of SAN cells

SAN cells were isolated as described previously (Mangoni and Nargeot, 2001). WT and $Girk4^{-/-}$ mice were killed by cervical dislocation under general anesthesia consisting of 0.01 mg/g xylazine (2% Rompun; Bayer AG) and 0.1 mg/g ketamine (Imalgène; Merial), and beating hearts were quickly removed. The SAN region was excised in warmed (35°C) Tyrode's solution containing (in mM): 140.0 NaCl, 5.4 KCl, 1.8 $CaCl_2$, 1.0 $MgCl_2$, 5.0 HEPES-NaOH, and 5.5 D-glucose (adjusted to pH 7.4 with NaOH) and cut in tissue strips. Strips were then transferred into a low-Ca^{2+}, low-Mg^{2+} solution containing (in mM): 140.0 NaCl, 5.4 KCl, 0.5 $MgCl_2$, 0.2 $CaCl_2$, 1.2 KH_2PO_4, 50.0 taurine, 5.5 D-glucose, 1.0 mg/ml BSA, and 5.0 HEPES-NaOH (adjusted to pH 6.9 with NaOH). The tissue was enzymatically digested by adding 229 U/ml collagenase type II (Worthington Biochemical Corporation), 1.9 U/ml elastase (Boehringer Mannheim), 0.9 U/ml protease (Sigma-Aldrich), 1 mg/ml BSA, and 200 µM $CaCl_2$. Tissue digestion was performed for a variable time of 9–13 min at 35°C with manual agitation using a flame-forged Pasteur pipette. Tissue strips were then washed and transferred into a medium containing (in mM): 70.0 L-glutamic acid, 20.0 KCl, 80.0 KOH, 10.0 (±) D-β-OH-butyric acid, 10.0 KH_2PO_4, 10.0 taurine, 1 mg/ml BSA, and 10.0 HEPES-KOH, pH 7.4 with KOH. SAN cells were manually dissociated in KB solution at 35°C for ∼10 min. Cellular automaticity was recovered by readapting the cells to physiological extracellular Na^+ and Ca^{2+} concentrations by adding aliquots of solutions containing (in mM): 10.0 NaCl, 1.8 $CaCl_2$, and, subsequently, normal Tyrode's solution containing 1 mg/ml BSA. The final storage solution contained (in mM): 100.0 NaCl, 35.0 KCl, 1.3 $CaCl_2$, 0.7 $MgCl_2$, 14.0 L-glutamic acid, 2.0 (±)D-β-OH-butyric acid, 2.0 KH_2PO_4, 2.0 taurine, and 1.0 mg/ml BSA, pH 7.4. Cells were then stored at room temperature until use. All chemicals were obtained from Sigma-Aldrich, except for the (±)D-β-OH-butyric acid, which was purchased from Fluka Chemika. For electrophysiological recording, SAN cells in the storage solution were harvested in special custom-made recording plexiglass chambers

with glass bottoms for proper cell attachment. The storage solution was continuously rinsed with normal Tyrode's solution warmed at 36°C before recording.

Patch-clamp recordings of mouse SAN cells

The basal extracellular Tyrode's solution used in all recordings contained (in mM): 140.0 NaCl, 5.4 KCl, 1.8 $CaCl_2$, 1.0 $MgCl_2$, 5.0 HEPES-NaOH, 5.5 and D-glucose (adjusted to pH 7.4 with NaOH). I_{KACh} and I_f were recorded using the standard whole-cell configuration. Patch-clamp electrodes had a resistance of 4–5 MΩ when filled with an intracellular solution containing (in mM): 130.0 K^+-aspartate; 10.0 NaCl; 2.0 ATP-Na^+ salt, 6.6 creatine phosphate, 0.1 GTP-Mg^{2+}, 0.04 $CaCl_2$ (pCa = 7.0), and 10.0 HEPES-KOH (adjusted to pH 7.2 with KOH). For recording $I_{Ca,L}$, K^+-aspartate in the intracellular solution was replaced with an equal amount of CsCl. The extracellular solution contained (in mM) 130 TEA-Cl, 2 $CaCl_2$, 1 $MgCl_2$, 10 4-amino-pyridine, and 25 HEPES (adjusted to pH 7.4 with TEA-OH). A correction of 9.8 mV because of liquid junction potential was applied in $I_{Ca,L}$ recordings (calculated with Patcher's Power Tools; Wavemetrics). All experiments were performed at 36°C. Pacemaker activity of SAN cells was recorded under perforated patch conditions by adding 50 µM β-escin to the pipette solution.

Isolated Langendorff perfused intact hearts

Excised hearts were quickly mounted on a Langendorff apparatus (Isolated heart system; EMKA Technologies) at a constant pressure of 80 mm Hg with normal Tyrode's solution. Perfused hearts were immersed in the water-jacked bath and maintained at 36°C. The electrocardiogram (ECG) was continuously recorded by Ag-AgCl electrodes positioned on the epicardial side of the right atrium close to the SAN area and near the apex. The heart rate was allowed to stabilize for at least 30 min before perfusion of ACh and/or isoproterenol (ISO).

Telemetric recordings of ECG and analysis

For telemetric ECG recording, adult male mice were anesthetized with 2% isoflurane. A midline incision was made on the back along the spine to insert a telemetric transmitter allowing simultaneous recording of ECG and home-cage activity (TA10EA-F20; Data Sciences International) into a subcutaneous pocket with paired wire electrodes placed over the thorax (chest bipolar ECG lead). Local anesthesia was obtained with 1% lidocaine injected subcutaneously at the sites of electrodes and transmitter implantation. To manage possible post-surgery pain, Advil (7 ml/l paracetamol and ibuprofen) was added to the drinking water for 4 d after implantation. Experiments were initiated at least 8 d after recovery from surgical implantation. Mice were housed in individual cages with ad libitum access to food and water and were exposed to standard 12-h light–dark cycles in a thermostatically controlled room. ECG signals were recorded using a telemetry receiver and an analogue to digital conversion data acquisition system for display and analysis by Dataquest A.R.T.TM software (Data Sciences International). Heart rates were determined from inter-beat (RR) intervals of the ECG. Mean heart rate values were obtained in each mouse for an overall 24-h period from 8:30 a.m. to 8:30 p.m. and analyzed as previously described by Alig et al. (2009). Heart rate variability (HRV) spectra of WT and $Girk4^{-/-}$ mice were analyzed from RR intervals according to Wickman et al. (1998). For drug administration or physical exercise experiments, mean heart rate values were calculated in each mouse by analyzing 5-min periods. ECG parameters were measured with ECG Auto 1.5.7 software.

Swimming tests were performed by using homemade plexiglass boxes of 15 × 32 cm and of 13 cm in height filled with prewarmed water (32°C) 9 cm deep. For exercise experiments, we used a two-mouse treadmill (model LE8709; BioSeb). Recovery to resting heart rate was assessed as the time to recovery (τ_r) calculated by fitting experimental data according to the one-phase-decay equation: $y = e^{(-k \times t)}$, where y is the heart rate value in beats per minute (bpm) at a given time, t is time, and $k = 1/\tau_r$.

Statistical analysis

Two-way ANOVA was used for comparisons between genotypes and multiple ACh concentrations. When needed, Sidak's multiple comparisons test was performed. Unpaired Student's *t* test was used in all other analysis. Data are represented as the mean ± the SEM. Analysis was performed using Prism 6.0 (GraphPad Software).

Online supplemental material

The supplemental text describes the mRNA extraction and RT-PCR protocol. Fig. S1 shows the expression and distribution of Girk subunits in different mouse tissues by RT-PCR. Fig. S2 shows the heart rate variation in $Girk4^{-/-}$ mice after administration of atropine, propranolol, and atropine plus propranolol. Fig. S3 shows the recovery of heart rate in $Girk4^{-/-}$ mice after treadmill test or intraperitoneal injection of atropine. Table S1 shows the action potential parameters in WT and $Girk4^{-/-}$ SAN cells before and after perfusion of 0.003, 0.01, and 0.05 µM ACh. Online supplemental material is available at http://www.jgp.org/cgi/content/full/jgp.201310996/DC1.

RESULTS

Expression of Girk4 in mouse SAN

Atrial myocardium expresses Girk1 and Girk4 subunits. Loss of Girk4 abolishes I_{KACh} single channel openings in cell-attached and inside-out patches of atrial cells of $Girk4^{-/-}$ mice (Wickman et al., 1998). We thus studied the distribution of Girk4 immunoreactivity in the intact SAN connected to the right atrium by macro-confocal microscopy. To define unambiguously the position of the SAN territory, as well as SAN pacemaker cells within the intact SAN-atrium preparation in WT and $Girk4^{-/-}$ hearts, we used anti-HCN4 immunoreactivity as a specific marker of spontaneously active SAN cells (Yamamoto et al., 2006; Christoffels et al., 2010). Staining of the intact SAN showed that HCN4-positive pacemaker cells were present in the cranial pole of the SAN, close to its boundary with the crista terminalis, and that their distribution was particularly dense in the region of dominant pacemaking identified by Verheijck et al. (2001; Fig. 1 A, left). We did not observe differences in the abundance, distribution, or location of HCN4-positive cells in $Girk4^{-/-}$ SAN preparations.

Girk4 immunoreactivity was present in both the SAN and right atrium (Fig. 1 A, middle). In the SAN region, Girk4 and HCN4 immunoreactivity largely overlapped (Fig. 1 A, right). Close-up views of pacemaker cells within the SAN showed that HCN4 immunoreactivity localized along the myocyte plasmalemma as reported previously in mouse SAN (Fig. 1 B, left; Herrmann et al., 2011). Individual HCN4-positive cells within the SAN region of WT hearts showed strong membrane-associated Girk4 and Girk1 immunoreactivity (Fig. 1 B, middle and right). Girk4 and Girk1 immunoreactivity overlapped

with HCN4 in the field of view in WT SAN (Manders coefficient of 0.46 ± 0.04 for Girk4 and 0.5 ± 0.05 [$n = 5$] for Girk1 immunoreactivity). In contrast, Girk4$^{-/-}$ SAN preparations displayed HCN4-positive and Girk4-negative cells (Manders coefficient of 0.004 ± 0.02; $n = 3$). In agreement with the notion that Girk1 is not targeted to the membrane in the absence of Girk4, we failed to observe membrane-bound Girk1 immunoreactivity in Girk4$^{-/-}$ SAN cells (Fig. 1 B, right).

Because it is known that the SAN gene expression profile may include ion channel genes that are not expressed in atria or ventricles (Marionneau et al., 2005), we tested the potential expression and distribution of mRNA coding for Girk2 or Girk3 subunits in the mouse SAN by RT-PCR (Fig. S1 A). To compare the expression

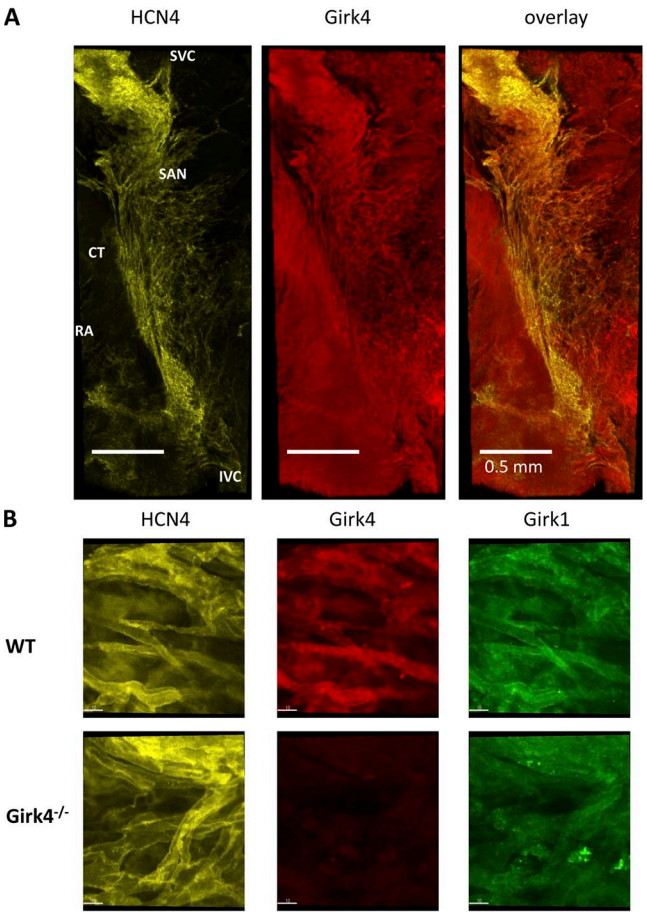

Figure 1. Distribution and localization of anti-Girk immunoreactivity in isolated mouse atrio-sinus preparations. (A) Representative images of $n = 3$ isolated SAN right atrium (RA) preparations (endocardial side) double stained with HCN4 and Girk4 antibodies. CT, crista terminalis; IVC and SVC, inferior and superior vena cava, respectively. (B) Close-up views of pacemaker cells within the SAN stained with HCN4, Girk4, or Girk1 antibodies. Individual HCN4-positive cells within the SAN region of WT hearts showed strong membrane-associated Girk4 and Girk1 immunoreactivity (top). Girk4$^{-/-}$ SAN cells displayed HCN4-positive and Girk4-negative staining and no membrane-bound Girk1 (bottom). Bars, 10 µm.

of Girk isoforms in cardiac and neuronal tissues, we purified mRNA from tissue samples of the SAN, right atrium, left ventricle, brain cortex, and cerebellum. Myocardial tissues and the SAN expressed only Girk4 and Girk1 mRNA, whereas Girk2 and Girk3 were expressed in the cortex and cerebellum, respectively. We did not find Girk4 mRNA in SAN preparations of Girk4$^{-/-}$ mice (Fig. S1).

Pacemaker cells from Girk4$^{-/-}$ mice lack I_{KACh}

We studied the expression of I_{KACh} current in WT and Girk4$^{-/-}$ SAN cells (Fig. 2). We recorded I_{KACh} by holding the membrane voltage at −35 mV and then perfusing ACh for 20 s before returning to control solution (Fig. 2 A). In WT cells, ACh dose-dependently increased the I_{KACh} current (Fig. 2, A and B). At concentrations of ACh >1 µM, the peak I_{KACh} current decreased as the result of channel desensitization (Fig. 2 B; Boyett and Roberts, 1987; Zang et al., 1993). We failed to observe detectable residual I_{KACh} in Girk4$^{-/-}$ SAN cells in the full range of ACh concentrations tested (Fig. 2, A and B). We also did not observe I_{KACh} in atrial cells that were isolated in parallel from the same Girk4$^{-/-}$ hearts used for recordings of SAN cells (not depicted). We conclude that inactivation of Girk4 channels abolished I_{KACh} in mouse SAN pacemaker cells.

We also tested whether inactivation of Girk4 affected the density of I_f and $I_{Ca,L}$, which are potentially involved in parasympathetic regulation of heart rate (Mangoni and Nargeot, 2008). We did not find significant difference in the peak densities, activation, and kinetics of I_f (Fig. 3 A) or $I_{Ca,L}$ (Fig. 3 B) between WT and in Girk4$^{-/-}$ SAN cells.

Loss of I_{KACh} in Girk4$^{-/-}$ mice reduces cholinergic regulation of pacemaker activity in SAN cells and in isolated intact hearts

To investigate how the loss of I_{KACh} affects the negative chronotropic effect of ACh on pacemaker activity, we recorded automaticity of SAN cells from WT and Girk4$^{-/-}$ mice (Fig. 4). To mimic moderate basal activation of the β-adrenergic signaling pathway, we added 2 nM ISO to the Tyrode's solution, a concentration inducing a submaximal positive chronotropic effect on SAN cell pacemaking (Alig et al., 2009). Under these conditions, the basal pacing rate, action potential threshold and duration, and maximum diastolic potential (MDP) of WT and Girk4$^{-/-}$ SAN cells did not significantly differ (Table S1). In WT cells, ACh dose-dependently slowed pacemaker activity, with effects evident at 0.003 µM and maximal at 0.05 µM (Fig. 4 A). At 0.003 µM, ACh-induced pacemaker rate reduction did not differ significantly between WT and Girk4$^{-/-}$ SAN cells, even though we observed a trend toward an increase in WT (17% in WT and 10% in Girk4$^{-/-}$ SAN cells; Fig. 4, A–C; and Table S1). At 0.01 µM ACh, the absence of Girk4 resulted

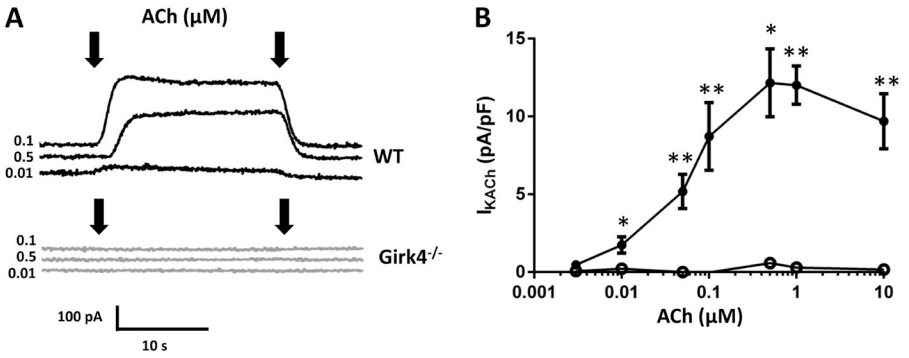

Figure 2. Inactivation of Girk4 channels ablates I_{KACh} in mouse SAN cells. (A) Sample traces of I_{KACh} current in WT and Girk4$^{-/-}$ SAN cells. I_{KACh} was activated by ACh in WT and Girk4$^{-/-}$ SAN cells. Arrows indicate the period of time for which ACh was added. (B) I_{KACh} density at different ACh concentrations in SAN cells from WT (0.003–10 μM; n = 4–16; closed circles) and Girk4$^{-/-}$ (0.003–10 μM; n = 3–13; open circles) mice. Error bars represent SEM. Statistical symbols: *, $P < 0.05$; and **, $P < 0.01$.

in an obvious difference in rate reduction, from 71% in WT to 36% in Girk4$^{-/-}$ SAN cells (Fig. 4, A–C). Finally, ACh induced a strong (52%) negative chronotropic effect on Girk4$^{-/-}$ SAN cells at 0.05 μM, but contrary to WT cells, we never observed cessation of pacemaker activity in knockout cells at this concentration. MDP was significant hyperpolarized in WT SAN cells challenged with 0.05 μM ACh (Fig. 4 A and Fig. S1 B); membrane hyperpolarization persisted for ∼4 s before settling to a stable membrane voltage that did not significantly differ from that recorded before ACh superfusion (Fig. S1 B). ACh reduced the slope of the diastolic depolarization in WT and Girk4$^{-/-}$ SAN cells at all concentrations >0.01 μM (Table S1). ACh did not affect the action potential threshold, velocity, duration, or MDP of WT and Girk4$^{-/-}$ SAN cells (Table S1).

We next investigated the impact of I_{KACh} ablation on the negative chronotropic effect of ACh in isolated Langendorff-perfused intact hearts (Fig. 5). At concentrations < 0.3 μM, ACh similarly slowed the beating rate of WT and Girk4$^{-/-}$ hearts (Fig. 5, A and B). Increasing ACh concentrations up to 10 μM dose-dependently reduced beating rates of WT hearts (53% decrease in beating rate). In contrast, the negative chronotropic response of Girk4$^{-/-}$ hearts to ACh at doses ranging from 0.3 to 10 μM did not significantly increase further (19%), indicating that loss of I_{KACh} induced saturation of the maximal negative chronotropic response at moderate

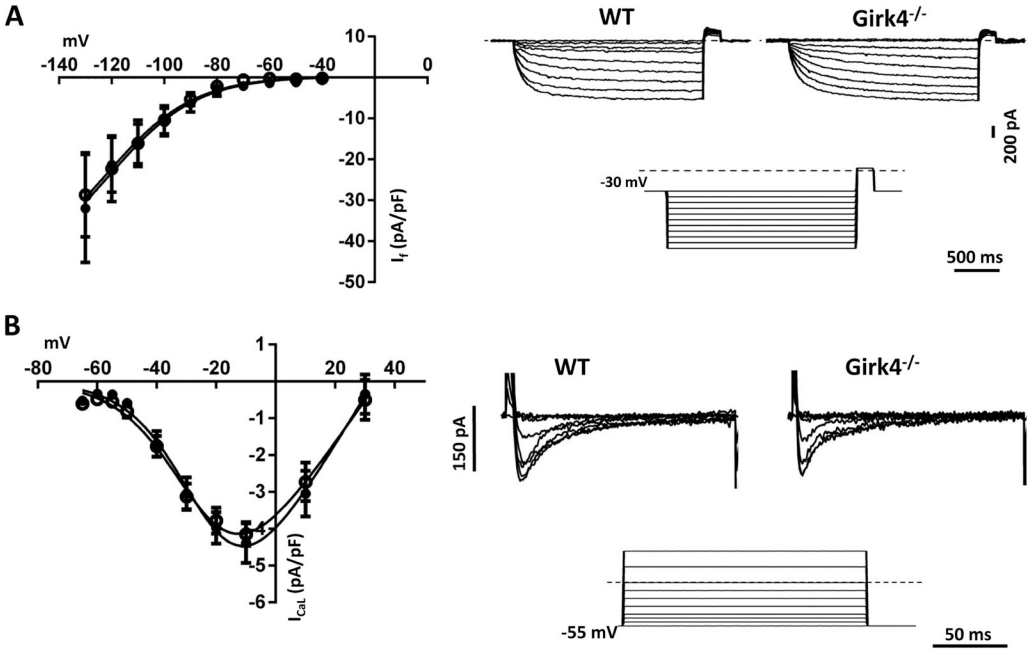

Figure 3. Loss of I_{KACh} in Girk4$^{-/-}$ mice did not affect functional expression of I_f and $I_{Ca,L}$. (A, left) Isochronal current to voltage curves for I_f in SAN cells from WT (n = 8; closed circles) and Girk4$^{-/-}$ (n = 10; open circles) mice. (right) Representative voltage-clamp recordings of I_f in isolated WT and Girk4$^{-/-}$ SAN cells. Applying hyperpolarizing voltage steps from a holding potential of −30 mV evoked I_f current. (B, left) Isochronal current to voltage curves of $I_{Ca,L}$ in SAN cells from WT (n = 12; closed circles) and Girk4$^{-/-}$ (n = 9; open circles). (right) Sample traces of $I_{Ca,L}$ in SAN cells from WT and Girk4$^{-/-}$ mice. Recordings were obtained by applying depolarizing voltage steps from a holding potential of −55 mV. Voltage-clamp protocols are shown below the traces, and the dashed lines indicate the zero voltage. Error bars represent SEM.

doses of ACh. Collectively, these observations indicate that I_{KACh} is an important determinant of cholinergic regulation of pacemaker activity in both isolated SAN cells and intact Langendorff-perfused hearts.

Heart rate regulation in Girk4$^{-/-}$ mice

To investigate the consequences of I_{KACh} ablation on heart rate regulation in vivo, we recorded ECGs of freely moving WT and Girk4$^{-/-}$ mice by telemetry (Fig. 6 A). WT and Girk4$^{-/-}$ mice had similar spontaneous activities in the home cage (not depicted; in agreement with previous observations), indicating that Girk4 inactivation does not affect locomotor activity (Wickman et al., 2000). Although there was normal high-frequency variation of heart rate (HRV) in WT, HRV in Girk4$^{-/-}$ mice varied on a slower time scale (Fig. 6, B and C). Consistent with previous observations in Girk4$^{-/-}$ mice of pure 129Sv/J or mixed (129Sv/J/C57B6/J) genetic backgrounds (Wickman et al., 1998), both the high- and low-frequency spectral components of HRV were reduced in our Girk4$^{-/-}$ mice (Fig. 6, D and E; Wickman et al., 1998).

We recorded significantly higher heart rates in Girk4$^{-/-}$ mice in comparison with that of WT mice over a typical 24-h recording period (Fig. 6, F–J). Indeed, the distribution of heart rates of Girk4$^{-/-}$ mice was shifted to higher values (Fig. 6 F), and elevated heart rate in Girk4$^{-/-}$ mice was present at all degrees of spontaneous activity in the home cage (Fig. 6 G). The rate to activity relationship of Girk4$^{-/-}$ mice was similar to that of WT counterparts (Fig. 6 G), indicating that mild tachycardia was caused by a reduced cholinergic response of SAN pacemaker activity rather than by an elevation of sympathetic tone in knockout animals. In agreement with this hypothesis, we observed similar increases in heart rate for any increase in spontaneous activity in WT and Girk4$^{-/-}$ mice (Fig. 6 H). Also, the difference between averaged maximal and minimal daily heart rates was similar in WT and Girk4$^{-/-}$ mice, demonstrating that, in spite of reduced HRV, the relative degree of

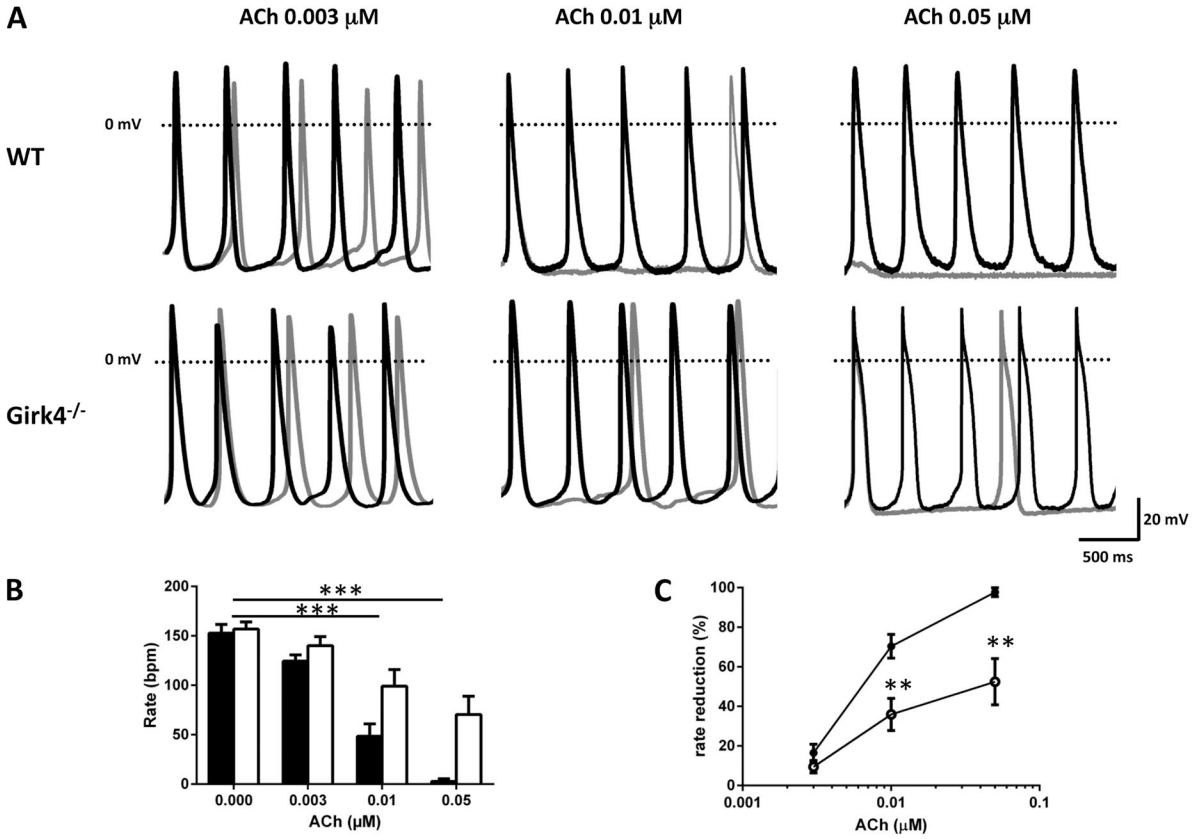

Figure 4. Cholinergic regulation of pacemaker activity in WT and Girk4$^{-/-}$ SAN cells. (A) Examples of spontaneous action potentials recorded in SAN cells from WT and Girk4$^{-/-}$ hearts in control conditions (black traces) and after perfusion of ACh (gray traces) at the indicated doses. (B) Histograms of pacing rate of WT (closed bars) and Girk4$^{-/-}$ (open bars) SAN cells in control conditions (WT $n = 6$; Girk4$^{-/-}$ $n = 6$) and after perfusion of 0.003 (WT $n = 5$; Girk4$^{-/-}$ $n = 7$), 0.01 (WT $n = 18$; Girk4$^{-/-}$ $n = 10$), and 0.05 μM ACh (WT $n = 5$; Girk4$^{-/-}$ $n = 7$). (C) Dose–response relation of the percentage of slowing of pacemaker rate by ACh in WT (closed circles) and Girk4$^{-/-}$ (open circles) SAN cells. At 0.01 μM ACh, inactivation of Girk4 channels significantly reduced the negative chronotropic effect from 67% in WT to 26% in Girk4$^{-/-}$ SAN cells. At 0.05 μM ACh, pacing was absent in WT, whereas it was reduced to ∼50% in Girk4$^{-/-}$ SAN cells. Error bars represent SEM. Statistical symbols: **, $P < 0.01$; and ***, $P < 0.001$.

regulation of daily heart rate was conserved after I_{KACh} ablation (Fig. 6, I and J).

To further test whether elevated heart rate in knockout mice was caused by loss of function of I_{KACh} in the SAN, we measured heart rates after systemic administration (intraperitoneally) of atropine or propranolol. We recorded similar heart rates in WT and Girk4$^{-/-}$ mice after inhibition of vagal input by administration of atropine, an observation which showed that sympathetic tone was not altered in Girk4$^{-/-}$ mice (Table 1, A and B, and Fig. S2). Similar heart rates were also observed after blockade of sympathetic input by propranolol or combined injection of these two drugs, indicating that vagal tone did not differ between WT and Girk4$^{-/-}$ mice (Table 1, A and B, and Fig. S2). These observations indicate that increased heart rates of Girk4$^{-/-}$ mice could not be ascribed to dysfunction of the sympathetic or vagal branches of the autonomic nervous system (Fig. S2). Furthermore, we did not observe significant differences in other parameters of the ECG waveform in comparing Girk4$^{-/-}$ mice with their WT counterparts (Table 1, A and B, and Fig. S2).

Next, we studied the effects of I_{KACh} loss in heart rate regulation under conditions of forced physical exercise. First, we recorded heart rate during a period of stress associated with physical activity (forced swim; Kirchhof et al., 2003; Harzheim et al., 2008). Heart rate was measured during a fixed exercise period, consisting of 5 min of swimming followed by 4 h of rest to recover basal heart rate in the home cage (Kirchhof et al., 2003). Both WT and Girk4$^{-/-}$ mice reached similar maximal heart rates during the 5-min swimming period (Fig. 7 A). However, WT mice returned to resting heart rates more rapidly than Girk4$^{-/-}$ mice; heart rates of WT mice reached resting levels after ∼55 min (τ_r = 33 ± 7 min), whereas >100 min were necessary for Girk4$^{-/-}$ mice to recover resting heart rates (τ_r = 58 ± 5 min; Fig. 7 A, inset). Similarly, on treadmill tests (Herrmann et al., 2007), WT and Girk4$^{-/-}$ mice ran for 5 min followed by a 4-h resting period. Similar to what was observed during the swimming test, knockout mice exhibited longer time to recovery of resting heart rates than their WT counterparts (τ_r = 17 ± 2 min in n = 6 WT and τ_r = 41 ± 11 min in n = 4 Girk4$^{-/-}$ mice; P < 0.05; Fig. S3 A).

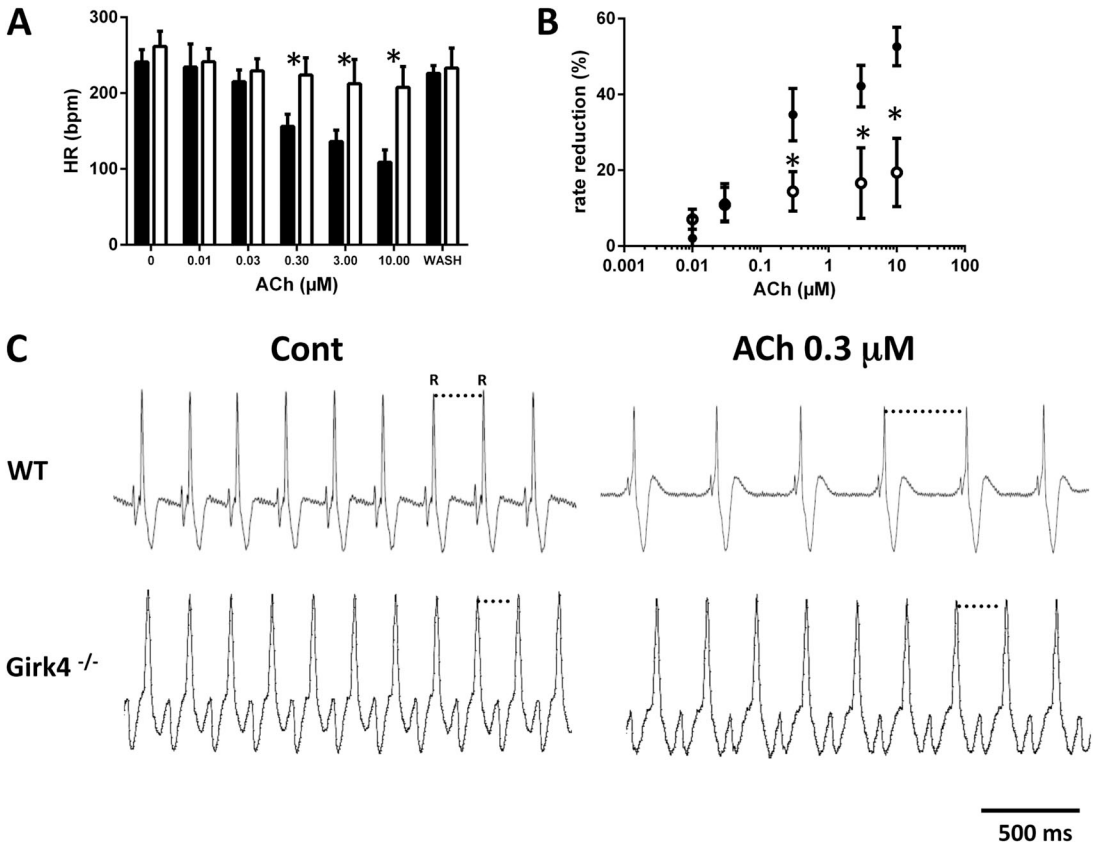

Figure 5. Negative chronotropic response to ACh of isolated WT and Girk4$^{-/-}$ hearts. (A and B) Dose–response relations expressed as absolute values (bpm; A) or percentage of heart rate (HR) slowing (B) by ACh in n = 7 WT (closed bars and circles) and n = 8 Girk4$^{-/-}$ Langendorff-perfused hearts (open bars and circles). (C) Sample traces of ECGs recorded from Langendorff-perfused hearts at baseline and after 0.3 µM ACh in WT and Girk4$^{-/-}$. Note that reduction in heart rate was more pronounced in WT than in Girk4$^{-/-}$ hearts. Error bars represent SEM. Statistical symbols: *, P < 0.05.

To test whether the difference in heart rate recovery could be reproduced by direct pharmacological activation of β-adrenergic receptors, we investigated the responsiveness of heart rate in vivo after systemic administration of 0.1 mg/kg ISO. Similar to what we observed with physical activity, WT and Girk4$^{-/-}$ mice reached comparable maximal heart rates after injection of ISO. Again, recovery of basal heart rate after ISO injection was longer in Girk4$^{-/-}$ than in WT mice (Fig. 7 B). In contrast, injection of atropine, which elevates heart rate by blocking muscarinic receptors, similarly increased heart rates in WT and Girk4$^{-/-}$ mice, but the recovery of basal heart rate did not differ significantly in the two mouse strains (Fig. S3 B).

We then investigated whether the delay in basal heart rate recovery observed in Girk4$^{-/-}$ mice could also be recorded in isolated hearts (Fig. 8 A). Because it was possible that β-adrenergic tone could persist, we recorded the time course of the ACh-mediated negative chronotropic effect under persistent β-adrenergic activation (Fig. 8 B). Our assumption was that this condition could mimic in vivo heart rate reduction by strong vagal activation in the presence of a persistent background β-adrenergic activation (Fig. 8 B). We paced isolated Langendorff-perfused WT and Girk4$^{-/-}$ hearts with 0.1 µM ISO for 5 min to allow the agonist effect to reach steady-state (Fig. 8 A). We then switched the perfusate to a test solution lacking ISO but containing

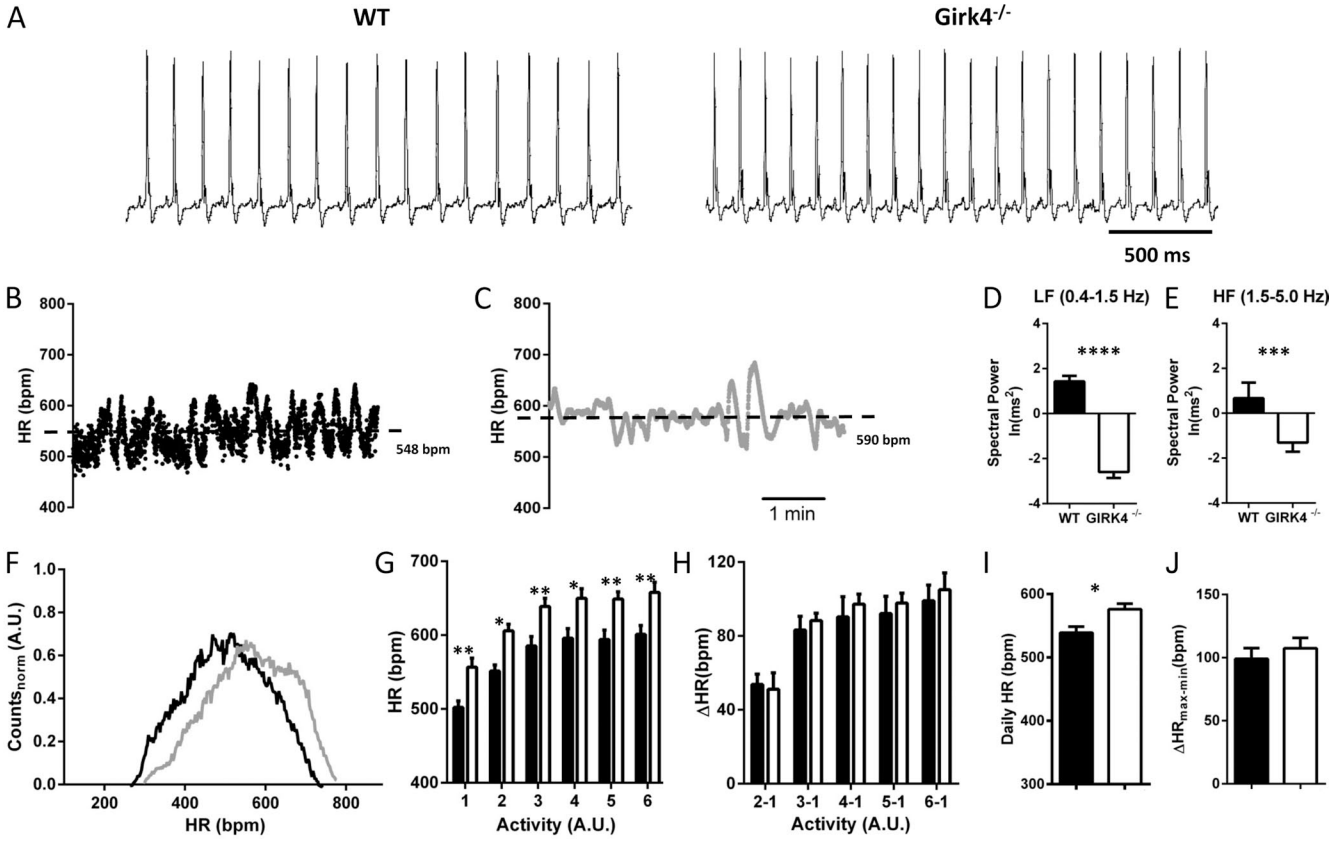

Figure 6. Heart rate in Girk4$^{-/-}$ mice. (A) Sample traces of ECGs recorded in freely moving WT and Girk4$^{-/-}$ mice. (B and C) Dot plots of beat to beat variability (in bpm) of heart rate (HR) of WT (B) and Girk4$^{-/-}$ (C) mice for a 5-min ECG recording epoch. The dashed lines indicate the averaged heart rate. (D and E) Bar graphs showing averaged low-frequency (LF; D) and high-frequency (HF; E) power spectra of HRV in WT (n = 10) and Girk4$^{-/-}$ (n = 9) mice for recordings shown in B and C. (F) Histogram showing the distribution of normalized averaged heart rates in a 24-h period of telemetric ECG recordings in WT (n = 10; black line) and Girk4$^{-/-}$ (n = 9; gray line) mice. For a given mouse, individual heart rate values were calculated every 20 s over the 24-h recording and then normalized to the maximal heart rate recorded for the mouse to allow comparison between WT and Girk4$^{-/-}$ animals. Note that the two distributions have similar shapes, but that Girk4$^{-/-}$ heart rates are shifted toward higher values. (G) Relationship between heart rate and spontaneous home cage activity (rate to activity relationship) of WT (closed bars) and Girk4$^{-/-}$ mice (open bars). Activity values are defined as arbitrary units (A.U.) and have been binned in six intervals of increasing activity. Binning was adjusted to obtain maximal resolution of the heart rate to activity relationship. (H) Similarity in the range of heart rate regulation as a function of activity in WT and Girk4$^{-/-}$ mice. For each animal, the heart rate corresponding to bin 1 (lowest activity) was subtracted from the heart rate recorded at other degrees of activity. (I) Averaged heart rate measured over a 24-h recording in Girk4$^{-/-}$ (583 ± 11 bpm; n = 9; open bars) and WT mice (539 ± 10 bpm; n = 10; closed bars; $P < 0.05$). (J) Range of heart rate regulation calculated from the differences between the maximum and minimum heart rate in each mouse recorded over the 24-h recording period. Error bars represent SEM. Statistical symbols: *, $P < 0.05$; **, $P < 0.01$; ***, $P < 0.001$; and ****, $P < 0.0001$.

TABLE 1 A

ECG interval values

Conditions	PR	QT	QRS	QTc
	ms	*ms*	*ms*	*ms*
WT_{NaCl}	38 ± 1	47 ± 2	11 ± 1	44 ± 2
$Girk4^{-/-}{}_{NaCl}$	36 ± 1	49 ± 2	11 ± 1	47 ± 2
WT_{Atrop}	34 ± 1	43 ± 3	10 ± 1	45 ± 2
$Girk4^{-/-}{}_{Atrop}$	34 ± 1	44 ± 2	11 ± 1	46 ± 2
WT_{Prop}	40 ± 2	55 ± 2	10 ± 1	42 ± 1
$Girk4^{-/-}{}_{Prop}$	41 ± 1	51 ± 2	10 ± 1	45 ± 2

See legend below Table 1 B.

0.3 µM ACh and observed the recovery of heart rate to the unstimulated condition before ISO perfusion (Fig. 8 A). Similarly to what we observed in freely moving mice, recovery of $Girk4^{-/-}$ hearts was significantly delayed in comparison with their WT counterparts (τ_r = 23 ± 10 s in n = 8 WT and τ_r = 101 ± 27 s in n = 7 $Girk4^{-/-}$ mice; $P < 0.05$; Fig. 8 A, inset). We then studied the time course of heart rate change upon perfusion of ACh under continuous stimulation by ISO. Under these conditions, ACh slowed pacing of ISO-stimulated WT and $Girk4^{-/-}$ hearts to a similar degree (54 ± 28 bpm and 59 ± 19 bpm in WT and $Girk4^{-/-}$ hearts, respectively; $P > 0.05$), but the pacemaker rate of knockout hearts reached steady-state levels after a significantly slower time course (τ_r = 24 ± 3 s in n = 8 WT and τ_r = 84 ± 12 s in n = 6 $Girk4^{-/-}$ mice; $P < 0.05$; Fig. 8 B, inset). Collectively, these observations indicate that the delay in heart rate recovery in $Girk4^{-/-}$ mice is a direct consequence of SAN I_{KACh} ablation.

DISCUSSION

We demonstrate that I_{KACh} is a critical mechanism involved in the muscarinic regulation of SAN pacemaker activity and heart rate regulation after the fight or flight response. Cardiac pacemaker activity is tightly regulated by the autonomic nervous system. Distinct ion channels or intracellular Ca^{2+} handling mechanisms are potentially involved in the parasympathetic control of pacemaker activity and heart rate, but their importance under different physiological conditions is still a matter of debate (Mangoni and Nargeot, 2008; DiFrancesco, 2010; Lakatta et al., 2010). In particular, the physiological importance of I_{KACh} in the autonomic regulation of SAN pacemaking is not completely understood. In atrial myocardium, I_{KACh} plays an important role in regulating resting membrane potential and action potential repolarization (Kaibara et al., 1991; Lomax et al., 2003). I_{KACh} activation also favors atrial reentry and triggering of atrial fibrillation by rapid pacing in experimental mammals (Cha et al., 2006) and mice (Kovoor et al., 2001). Selective block of I_{KACh} prevents ACh-induced conduction block in the AV node, demonstrating that this current plays an important role in vagal regulation of atrioventricular conduction (Drici et al., 2000). Even if Girk1 and Girk4 subunits are relatively poorly expressed in ventricular tissue in comparison with atrium (Dobrzynski et al., 2001), I_{KACh} can exert a direct negative inotropic effect in ventricular myocytes (McMorn et al., 1993), suggesting that this current also regulates the ventricular and Purkinje fiber action potentials in some species.

Here, we showed that genetic inactivation of I_{KACh} strongly diminishes the cholinergic regulation of SAN pacemaking and reduces the speed of recovery of resting heart rates after physiological tests mimicking the fight or flight response. The expression profile of Girk channel subunits in the mouse SAN is similar to that of the atria (Wickman et al., 1998). No mRNA coding for Girk2 or Girk3 subunits could be amplified in PCR

TABLE 1 B

Statistical analysis of RR and PR ECG intervals

Conditions	RR/PR				
	$Girk4^{-/-}{}_{NaCl}$	WT_{Atrop}	$Girk4^{-/-}{}_{Atrop}$	WT_{Prop}	$Girk4^{-/-}{}_{Prop}$
WT_{NaCl}	NS/NS	<0.05/NS	<0.01/<0.05	<0.01/NS	<0.001/NS
$Girk4^{-/-}{}_{NaCl}$		NS/NS	<0.05/NS	<0.001/NS	<0.001/<0.01
WT_{Atrop}			NS/NS	<0.001/<0.01	<0.001/<0.001
$Girk4^{-/-}{}_{Atrop}$				<0.001/<0.001	<0.001/<0.001
WT_{Prop}					NS/NS

Atrop, atropine; Prop, propranolol. ECG interval values in WT and $Girk4^{-/-}$ mice under control conditions (intraperitoneal injection of NaCl) or after systemic administration of 0.5 mg/kg atropine or 5 mg/kg propranolol are shown.

experiments of SAN tissue (Fig. S1 A). In contrast, Girk4 immunoreactivity was widely distributed in the SAN, defined as the HCN4-positive region bordered by the caval veins, the crista terminalis, and the interatrial septum (Yamamoto et al., 2006). SAN cells expressing anti-HCN4 immunoreactivity were also positive for Girk4 and Girk1, with strong membrane-bound protein expression as described in larger mammals (Dobrzynski et al., 2001). We did not observe residual positive anti-Girk4 immunoreactivity in individual SAN cells within the intact SAN of Girk4$^{-/-}$ hearts. Although SAN cells from knockout hearts exhibited Girk1 immunoreactivity, staining did not appear to be associated with cell membranes. This observation is consistent with the notion that Girk1 subunits cannot form functional channels in the absence of Girk4 (Kennedy et al., 1999) and that atrial myocytes isolated from Girk4$^{-/-}$ mice do not have residual I_{KACh} channel activity (Wickman et al., 1998). Accordingly, we failed to observe residual I_{KACh} in SAN cells of Girk4$^{-/-}$ mice (Fig. 2).

I_{KACh} loss of function strongly reduced the negative chronotropic effect of ACh in both isolated SAN cells and intact Langendorff-perfused hearts. The pacemaker activity of isolated SAN cells was more sensitive to ACh than that of intact hearts. This difference may result from the "pacemaker shift" phenomenon, in which perfusion of ACh shifts the dominant site of origin of the SAN impulse to groups of cells with lower sensitivity to ACh (Boyett et al., 2000). Remarkably, the maximal negative chronotropic effect induced by high doses of ACh (0.3–10 μM) in Girk4$^{-/-}$ hearts did not exceed 20%, whereas WT hearts slowed pacemaking by ∼35–53%. At relatively low agonist concentrations (<0.3 μM), the ACh-induced negative chronotropic effect was similar between WT and Girk4$^{-/-}$ mice, but heart rate slowing was modest or moderate (5–10%). In this respect, it has been proposed that the muscarinic regulation of heart rate at low vagal tone or ACh concentration depends exclusively on I_f (DiFrancesco et al., 1989; Zaza et al., 1996; Yamada, 2002). It is thus possible that

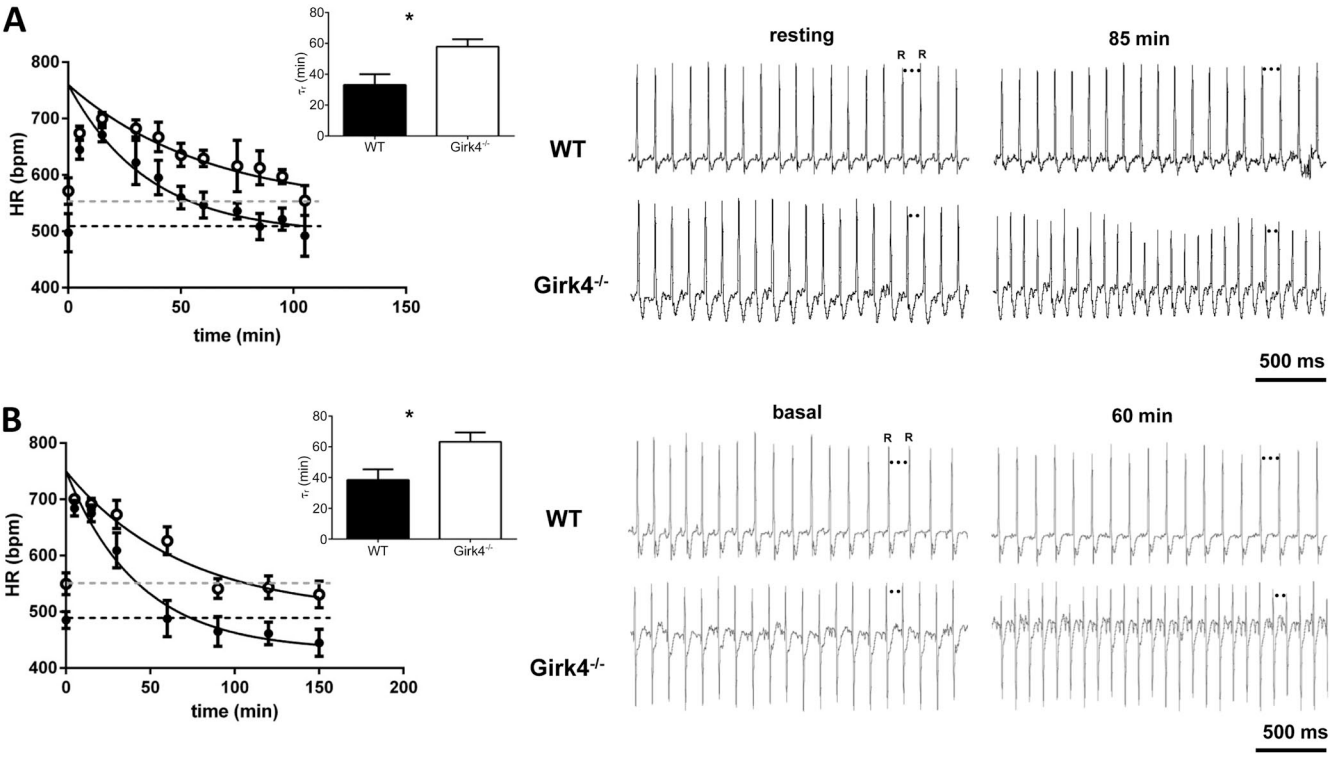

Figure 7. Recovery of resting heart rate in Girk4$^{-/-}$ mice. (A and B) After swimming test (A) and upon intraperitoneal injection of ISO (B). (A, left) Swimming test (5 min) was used to monitor heart rate (HR) during physical exercise of WT (n = 5; closed circles) and Girk4$^{-/-}$ (n = 6; open circles) mice. Continuous lines represent fitting of experimental data points to calculate τ_r of recovery. Dashed lines represent the basal heart rate before swimming test in WT (black) and Girk4$^{-/-}$ (gray) mice. Averaged τ_r for WT and Girk4$^{-/-}$ mice is reported in the insets. (right) Samples ECG traces from WT and Girk4$^{-/-}$ mice at rest (before swimming) and 85 min after swimming. Note that at 85 min in Girk4$^{-/-}$ but not in WT mice, heart rate was still higher than the heart rate in the resting condition. (B, left) Basal heart rate recovery after direct activation of β-adrenergic receptors by 0.1 mg/kg ISO in WT (n = 15; closed circles) and Girk4$^{-/-}$ (n = 11; open circles) mice. Dashed lines represent the basal heart rate before injection of ISO in WT (black) and Girk4$^{-/-}$ (gray) mice. Averaged τ_r for WT and Girk4$^{-/-}$ mice is reported in the inset. (right) Samples ECG traces from WT and Girk4$^{-/-}$ mice under basal conditions and 60 min after ISO injection. At min 60 in Girk4$^{-/-}$ mice but not in WT, heart rate was still higher than the basal heart rate. Error bars represent SEM. Statistical symbols: *, $P < 0.05$.

negative regulation of I_f current by ACh was responsible, at least in part, for the chronotropic effect observed at low agonist doses observed in our experiments.

The mean daily heart rate of Girk4$^{-/-}$ mice was significantly faster than that of WT mice, irrespective of the relative level of spontaneous activity. Resting heart rates recorded before drug administration or physical tests also showed a trend to elevation in knockout animals. It is important to note that in spite of increased basal heart rates and reduced HRV, the relative degree of rate regulation was similar in WT and Girk4$^{-/-}$ mice. In other words, despite the fact that Girk4$^{-/-}$ mice cannot adjust their heart rate on short time scales (Wickman et al., 1998), they can still exhibit fluctuations comparable with those measured in WT controls. This observation suggests that other mechanisms involved in autonomic regulation of SAN pacemaking, such as cAMP-dependent regulation of f-channels (DiFrancesco, 1993), $I_{Ca,L}$ (Petit-Jacques et al., 1993; Zaza et al., 1996; Mangoni et al., 2003), and ryanodine receptor–dependent Ca^{2+} release (Lyashkov et al., 2009; van Borren et al., 2010) can sustain a degree of vagal control of pacemaker activity in vivo.

Our experimental data indicate that moderate tachycardia is caused by a loss of tonic inhibition of SAN pacemaking by I_{KACh} rather than by sympathetic overdrive in knockout mice. First, the rate to activity relationships in WT and Girk4$^{-/-}$ mice were similar, with the degree of heart rate regulation preserved after increasing activity. This observation shows that Girk4$^{-/-}$ mice have a normal range of heart rate control and compliance of the autonomic nervous system. In this respect, the phenotype of Girk4$^{-/-}$ mice clearly differed from that of mice lacking voltage-dependent $Ca_v2.2$ Ca^{2+} channels, which show elevated heart rate as the result of increased sympathetic tone and have a strongly reduced range of cardiovascular control (Ino et al., 2001). Second, we recorded similar maximal heart rates and time to recovery of basal rate upon injection of atropine in WT and Girk4$^{-/-}$ mice, although

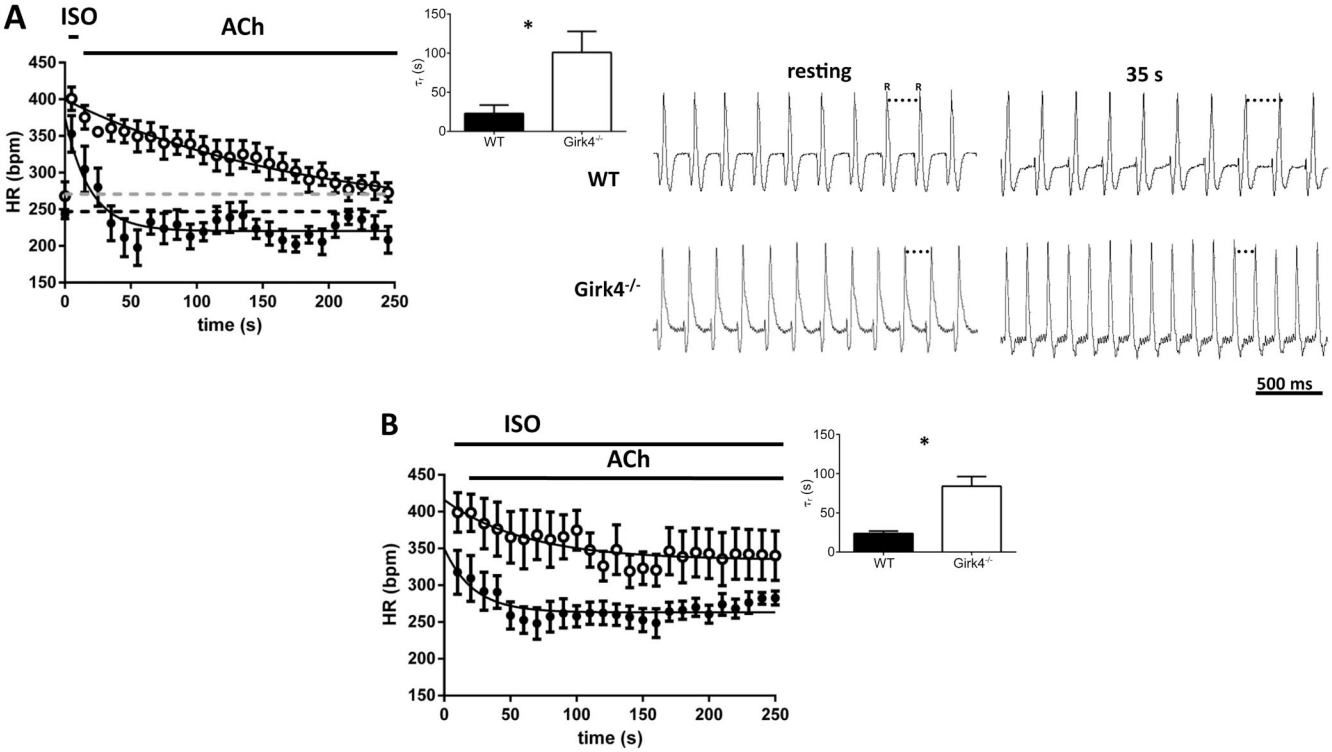

Figure 8. Recovery of resting heart rate in isolated WT and Girk4$^{-/-}$ hearts and time course of ACh-induced heart rate reduction under continuous ISO perfusion. (A, left) Basal heart rate (HR) recovery in 0.3 µM ACh after application of 0.1 µM ISO for 5 min in WT (n = 8; closed circles) and Girk4$^{-/-}$ (n = 7; open circles) Langendorff-perfused hearts. The first data point for each genotype represents heart rate under basal condition, whereas the second data point is the averaged maximal heart rate under ISO, before switching to the solution containing ACh. Dashed lines indicate the basal heart rate before ISO perfusion in WT (black) and Girk4$^{-/-}$ (gray) mice. Continuous lines represent fitting of experimental data points for calculating τ_r of recovery. Averaged τ_r for WT and Girk4$^{-/-}$ isolated hearts is shown in the insets. (right) Sample ECG traces from WT and Girk4$^{-/-}$ recorded in isolated hearts under resting conditions (before ISO) and 35 s after ACh application. Note that at 35 s in Girk4$^{-/-}$ but not in WT hearts, the pacing rate was still higher than at rest. (B) Similar to A, the first data point is the averaged maximal heart rate with ISO before perfusion. The time course (τ_r) of rate reduction was calculated during combined perfusion of 0.1 µM ISO and ACh 0.3 µM after maximal stimulation of pacing by ISO in WT (n = 8; closed circles) and Girk4$^{-/-}$ (n = 6; open circles) hearts. The inset shows averaged τ_r for WT and Girk4$^{-/-}$ hearts. Error bars represent SEM. Statistical symbols: *, $P < 0.05$.

higher heart rates and recovery times would have been expected in the presence of increased background sympathetic tone in knockout animals. Third, the slightly more pronounced effect of β-adrenergic receptor blockade on heart rates of knockout mice is consistent with the hypothesis of reduced muscarinic regulation of SAN pacemaking because the heart rate of WT and Girk4$^{-/-}$ mice should not differ under this condition. In addition, heart rates recorded under β-block should be similar to intrinsic heart hearts after complete autonomic block by combined injection of atropine and propranolol. Both of these conditions are experimentally verified in WT and Girk4$^{-/-}$ mice. Finally, WT and Girk4$^{-/-}$ mice showed similar PR intervals, an observation which shows that sympathetic tone was not appreciably changed in knockout animals.

I_{KACh} is a critical mechanism involved in recovery of resting heart rate upon stress, physical exercise, or direct pharmacological β-adrenergic activation. Several lines of evidence indicate that such a delay is directly caused by I_{KACh} loss of function in the heart and not by dysfunction of the autonomic nervous system branches. First, a slower time course in heart rate change could be observed in isolated hearts after maximal β-adrenergic stimulation of pacing rate or under conditions of accentuated antagonism. We did not find evidence of any constitutive reduction in the vagal tone of knockout mice because inhibition of β-adrenergic receptors negated the difference in basal heart rate between WT and Girk4$^{-/-}$ mice. Finally, slowed resting heart rate recovery in Girk4$^{-/-}$ mice was unlikely to be caused by alteration in ionic currents involved in vagal control of heart rate because we found similar I_f and $I_{Ca,L}$ densities in WT and Girk4$^{-/-}$ SAN cells. The possibility that Girk4$^{-/-}$ mice have major alterations in other ionic currents involved in automaticity is also unlikely because the intrinsic heart rate measured after combined injection of atropine and propranolol did not differ between WT and knockout animals.

The finding that I_{KACh} is an important mechanism of recovery to resting heart rate was unanticipated. We surmise that recovery of resting heart rate after sympathetic stimulation requires many minutes because down-regulation of cAMP and consequent dephosphorylation of membrane ion channels and/or intracellular Ca^{2+} handling proteins proceed on a slow time scale in the intact SAN. This hypothesis would be consistent with a previous study showing that inhibition of I_{KACh} with tertiapin reduced the negative chronotropic response to high-frequency vagal stimulation by >70% in rabbit hearts (Mizuno et al., 2007). Interestingly, delayed recovery to basal heart rates was observed also after the treadmill test, in which fear responses are less prominent than in swimming tests. This last observation renders it unlikely that the delayed recovery to resting heart rates in Girk4$^{-/-}$ mice is entirely caused by stress hormones. However, an additional possibility is that sympathetic tone remains elevated after stress or forced physical activity for relatively long periods and that I_{KACh} is an important mechanism to counteract this phenomenon.

We thank the staff of the RAM animal facility of Montpellier for managing the Girk4$^{-/-}$ mouse line and the staff of the Montpellier RIO imaging platform. We also thank Isabelle Bidaud for excellent technical assistance.

The project was supported by Agence Nationale pour la Recherche (ANR) grants ANR-06-PHISIO-004-01, ANR-2010-BLAN-1128-01, and ANR-09-GENO-034 (to M.E. Mangoni), by the Fondation de France (Cardiovasc 2008002730 to J. Nargeot), and by National Institutes of Health grants RO1HL087120-A2 (to M.E. Mangoni) and RO1 HL105550 (to K. Wickman). A.G. Torrente and P. Mesirca were supported by CavNet, a Research Training Network, funded through the European Union Research Programme (6FP) MRTN-CT-2006-035367. L. Marger is the recipient of a postdoctoral fellowship from the Fondation Lefoulon-Delalande. The Institut de Génomique Fonctionnelle group is a member of the Laboratory of Excellence Ion Channel Science and Therapeutics, supported by a grant from the ANR (ANR-11-LABX-0015).

Edward N. Pugh Jr. served as editor.

Submitted: 28 March 2013
Accepted: 20 June 2013

REFERENCES

Alig, J., L. Marger, P. Mesirca, H. Ehmke, M.E. Mangoni, and D. Isbrandt. 2009. Control of heart rate by cAMP sensitivity of HCN channels. *Proc. Natl. Acad. Sci. USA*. 106:12189–12194. http://dx.doi.org/10.1073/pnas.0810332106

Bolte, S., and F.P. Cordelières. 2006. A guided tour into subcellular colocalization analysis in light microscopy. *J. Microsc.* 224:213–232. http://dx.doi.org/10.1111/j.1365-2818.2006.01706.x

Boyett, M.R., and A. Roberts. 1987. The fade of the response to acetylcholine at the rabbit isolated sino-atrial node. *J. Physiol.* 393: 171–194.

Boyett, M.R., H. Honjo, and I. Kodama. 2000. The sinoatrial node, a heterogeneous pacemaker structure. *Cardiovasc. Res.* 47:658–687. http://dx.doi.org/10.1016/S0008-6363(00)00135-8

Cha, T.J., J.R. Ehrlich, D. Chartier, X.Y. Qi, L. Xiao, and S. Nattel. 2006. Kir3-based inward rectifier potassium current: potential role in atrial tachycardia remodeling effects on atrial repolarization and arrhythmias. *Circulation.* 113:1730–1737. http://dx.doi.org/10.1161/CIRCULATIONAHA.105.561738

Christoffels, V.M., G.J. Smits, A. Kispert, and A.F. Moorman. 2010. Development of the pacemaker tissues of the heart. *Circ. Res.* 106: 240–254. http://dx.doi.org/10.1161/CIRCRESAHA.109.205419

DiFrancesco, D. 1993. Pacemaker mechanisms in cardiac tissue. *Annu. Rev. Physiol.* 55:455–472. http://dx.doi.org/10.1146/annurev.ph.55.030193.002323

DiFrancesco, D. 2010. The role of the funny current in pacemaker activity. *Circ. Res.* 106:434–446. http://dx.doi.org/10.1161/CIRCRESAHA.109.208041

DiFrancesco, D., P. Ducouret, and R.B. Robinson. 1989. Muscarinic modulation of cardiac rate at low acetylcholine concentrations. *Science.* 243:669–671. http://dx.doi.org/10.1126/science.2916119

Dobrzynski, H., D.D. Marples, H. Musa, T.T. Yamanushi, Z. Henderson, Y. Takagishi, H. Honjo, I. Kodama, and M.R. Boyett. 2001. Distribution of the muscarinic K^+ channel proteins Kir3.1 and Kir3.4 in the ventricle, atrium, and sinoatrial node of heart. *J. Histochem. Cytochem.* 49:1221–1234. http://dx.doi.org/10.1177/002215540104901004

Drici, M.D., S. Diochot, C. Terrenoire, G. Romey, and M. Lazdunski. 2000. The bee venom peptide tertiapin underlines the role of I_{KACh} in acetylcholine-induced atrioventricular blocks. *Br. J. Pharmacol.* 131:569–577. http://dx.doi.org/10.1038/sj.bjp.0703611

Giles, W., and S.J. Noble. 1976. Changes in membrane currents in bullfrog atrium produced by acetylcholine. *J. Physiol.* 261:103–123.

Harzheim, D., K.H. Pfeiffer, L. Fabritz, E. Kremmer, T. Buch, A. Waisman, P. Kirchhof, U.B. Kaupp, and R. Seifert. 2008. Cardiac pacemaker function of HCN4 channels in mice is confined to embryonic development and requires cyclic AMP. *EMBO J.* 27:692–703. http://dx.doi.org/10.1038/emboj.2008.3

Herrmann, S., J. Stieber, G. Stöckl, F. Hofmann, and A. Ludwig. 2007. HCN4 provides a 'depolarization reserve' and is not required for heart rate acceleration in mice. *EMBO J.* 26:4423–4432. http://dx.doi.org/10.1038/sj.emboj.7601868

Herrmann, S., B. Layh, and A. Ludwig. 2011. Novel insights into the distribution of cardiac HCN channels: an expression study in the mouse heart. *J. Mol. Cell. Cardiol.* 51:997–1006. http://dx.doi.org/10.1016/j.yjmcc.2011.09.005

Ino, M., T. Yoshinaga, M. Wakamori, N. Miyamoto, E. Takahashi, J. Sonoda, T. Kagaya, T. Oki, T. Nagasu, Y. Nishizawa, et al. 2001. Functional disorders of the sympathetic nervous system in mice lacking the alpha 1B subunit (Cav 2.2) of N-type calcium channels. *Proc. Natl. Acad. Sci. USA.* 98:5323–5328. http://dx.doi.org/10.1073/pnas.081089398

Kaibara, M., T. Nakajima, H. Irisawa, and W. Giles. 1991. Regulation of spontaneous opening of muscarinic K^+ channels in rabbit atrium. *J. Physiol.* 433:589–613.

Kennedy, M.E., J. Nemec, S. Corey, K. Wickman, and D.E. Clapham. 1999. GIRK4 confers appropriate processing and cell surface localization to G-protein-gated potassium channels. *J. Biol. Chem.* 274:2571–2582. http://dx.doi.org/10.1074/jbc.274.4.2571

Kirchhof, P., L. Fabritz, L. Fortmuller, G.P. Matherne, A. Lankford, H.A. Baba, W. Schmitz, G. Breithardt, J. Neumann, and P. Boknik. 2003. Altered sinus nodal and atrioventricular nodal function in freely moving mice overexpressing the A1 adenosine receptor. *Am. J. Physiol. Heart Circ. Physiol.* 285:H145–H153.

Kovoor, P., K. Wickman, C.T. Maguire, W. Pu, J. Gehrmann, C.I. Berul, and D.E. Clapham. 2001. Evaluation of the role of I_{KACh} in atrial fibrillation using a mouse knockout model. *J. Am. Coll. Cardiol.* 37:2136–2143. http://dx.doi.org/10.1016/S0735-1097(01)01304-3

Krapivinsky, G., E.A. Gordon, K. Wickman, B. Velimirović, L. Krapivinsky, and D.E. Clapham. 1995. The G-protein-gated atrial K^+ channel I_{KACh} is a heteromultimer of two inwardly rectifying K^+-channel proteins. *Nature.* 374:135–141. http://dx.doi.org/10.1038/374135a0

Lakatta, E.G., V.A. Maltsev, and T.M. Vinogradova. 2010. A coupled SYSTEM of intracellular Ca^{2+} clocks and surface membrane voltage clocks controls the timekeeping mechanism of the heart's pacemaker. *Circ. Res.* 106:659–673. http://dx.doi.org/10.1161/CIRCRESAHA.109.206078

Löffelholz, K., and A.J. Pappano. 1985. The parasympathetic neuroeffector junction of the heart. *Pharmacol. Rev.* 37:1–24.

Lomax, A.E., R.A. Rose, and W.R. Giles. 2003. Electrophysiological evidence for a gradient of G protein-gated K^+ current in adult mouse atria. *Br. J. Pharmacol.* 140:576–584. http://dx.doi.org/10.1038/sj.bjp.0705474

Lyashkov, A.E., T.M. Vinogradova, I. Zahanich, Y. Li, A. Younes, H.B. Nuss, H.A. Spurgeon, V.A. Maltsev, and E.G. Lakatta. 2009. Cholinergic receptor signaling modulates spontaneous firing of sinoatrial nodal cells via integrated effects on PKA-dependent Ca^{2+} cycling and $I_{KACh.}$ *Am. J. Physiol. Heart Circ. Physiol.* 297:H949–H959. http://dx.doi.org/10.1152/ajpheart.01340.2008

Mangoni, M.E., and J. Nargeot. 2001. Properties of the hyperpolarization-activated current (I_f) in isolated mouse sino-atrial cells. *Cardiovasc. Res.* 52:51–64. http://dx.doi.org/10.1016/S0008-6363(01)00370-4

Mangoni, M.E., and J. Nargeot. 2008. Genesis and regulation of the heart automaticity. *Physiol. Rev.* 88:919–982. http://dx.doi.org/10.1152/physrev.00018.2007

Mangoni, M.E., B. Couette, E. Bourinet, J. Platzer, D. Reimer, J. Striessnig, and J. Nargeot. 2003. Functional role of L-type Cav1.3 Ca^{2+} channels in cardiac pacemaker activity. *Proc. Natl. Acad. Sci. USA.* 100:5543–5548. http://dx.doi.org/10.1073/pnas.0935295100

Marionneau, C., B. Couette, J. Liu, H. Li, M.E. Mangoni, J. Nargeot, M. Lei, D. Escande, and S. Demolombe. 2005. Specific pattern of ionic channel gene expression associated with pacemaker activity in the mouse heart. *J. Physiol.* 562:223–234. http://dx.doi.org/10.1113/jphysiol.2004.074047

McMorn, S.O., S.M. Harrison, W.J. Zang, X.J. Yu, and M.R. Boyett. 1993. A direct negative inotropic effect of acetylcholine on rat ventricular myocytes. *Am. J. Physiol.* 265:H1393–H1400.

Mizuno, M., A. Kamiya, T. Kawada, T. Miyamoto, S. Shimizu, and M. Sugimachi. 2007. Muscarinic potassium channels augment dynamic and static heart rate responses to vagal stimulation. *Am. J. Physiol. Heart Circ. Physiol.* 293:H1564–H1570. http://dx.doi.org/10.1152/ajpheart.00368.2007

Noma, A., and W. Trautwein. 1978. Relaxation of the ACh-induced potassium current in the rabbit sinoatrial node cell. *Pflugers Arch.* 377:193–200. http://dx.doi.org/10.1007/BF00584272

Pauza, D.H., V. Skripka, N. Pauziene, and R. Stropus. 1999. Anatomical study of the neural ganglionated plexus in the canine right atrium: implications for selective denervation and electrophysiology of the sinoatrial node in dog. *Anat. Rec.* 255:271–294. http://dx.doi.org/10.1002/(SICI)1097-0185(19990701)255:3<271::AID-AR4>3.0.CO;2-2

Pauza, D.H., V. Skripka, N. Pauziene, and R. Stropus. 2000. Morphology, distribution, and variability of the epicardiac neural ganglionated subplexuses in the human heart. *Anat. Rec.* 259:353–382. http://dx.doi.org/10.1002/1097-0185(20000801)259:4<353::AID-AR10>3.0.CO;2-R

Petit-Jacques, J., P. Bois, J. Bescond, and J. Lenfant. 1993. Mechanism of muscarinic control of the high-threshold calcium current in rabbit sino-atrial node myocytes. *Pflugers Arch.* 423:21–27. http://dx.doi.org/10.1007/BF00374956

van Borren, M.M., A.O. Verkerk, R. Wilders, N. Hajji, J.G. Zegers, J. Bourier, H.L. Tan, E.E. Verheijck, S.L. Peters, A.E. Alewijnse, and J.H. Ravesloot. 2010. Effects of muscarinic receptor stimulation on Ca^{2+} transient, cAMP production and pacemaker frequency of rabbit sinoatrial node cells. *Basic Res. Cardiol.* 105:73–87. http://dx.doi.org/10.1007/s00395-009-0048-9

Verheijck, E.E., M.J. van Kempen, M. Veereschild, J. Lurvink, H.J. Jongsma, and L.N. Bouman. 2001. Electrophysiological features of the mouse sinoatrial node in relation to connexin distribution. *Cardiovasc. Res.* 52:40–50. http://dx.doi.org/10.1016/S0008-6363(01)00364-9

Wickman, K.D., and D.E. Clapham. 1995. G-protein regulation of ion channels. *Curr. Opin. Neurobiol.* 5:278–285. http://dx.doi.org/10.1016/0959-4388(95)80039-5

Wickman, K., J. Nemec, S.J. Gendler, and D.E. Clapham. 1998. Abnormal heart rate regulation in GIRK4 knockout mice. *Neuron.* 20:103–114. http://dx.doi.org/10.1016/S0896-6273(00)80438-9

Wickman, K., G. Krapivinsky, S. Corey, M. Kennedy, J. Nemec, I. Medina, and D.E. Clapham. 1999. Structure, G protein activation, and functional relevance of the cardiac G protein-gated K^+ channel, $I_{KACh.}$ *Ann. N. Y. Acad. Sci.* 868:386–398. http://dx.doi.org/10.1111/j.1749-6632.1999.tb11300.x

Wickman, K., C. Karschin, A. Karschin, M.R. Picciotto, and D.E. Clapham. 2000. Brain localization and behavioral impact of the G-protein-gated K^+ channel subunit GIRK4. *J. Neurosci.* 20:5608–5615.

Yamada, M. 2002. The role of muscarinic K^+ channels in the negative chronotropic effect of a muscarinic agonist. *J. Pharmacol. Exp. Ther.* 300:681–687. http://dx.doi.org/10.1124/jpet.300.2.681

Yamamoto, M., H. Dobrzynski, J. Tellez, R. Niwa, R. Billeter, H. Honjo, I. Kodama, and M.R. Boyett. 2006. Extended atrial conduction system characterised by the expression of the HCN4 channel and connexin45. *Cardiovasc. Res.* 72:271–281. http://dx.doi.org/10.1016/j.cardiores.2006.07.026

Zang, W.J., X.J. Yu, H. Honjo, M.S. Kirby, and M.R. Boyett. 1993. On the role of G protein activation and phosphorylation in desensitization to acetylcholine in guinea-pig atrial cells. *J. Physiol.* 464:649–679.

Zaza, A., R.B. Robinson, and D. DiFrancesco. 1996. Basal responses of the L-type Ca^{2+} and hyperpolarization-activated currents to autonomic agonists in the rabbit sino-atrial node. *J. Physiol.* 491:347–355.